Towards the Calibration of the HETGS Line Response Function

H.L. Marshall, D. Dewey, K.A. Flanagan, C. Baluta, C.R. Canizares, D.S. Davis, J.E. Davis, T.T. Fang, D.P. Huenemoerder, J.H. Kastner, N.S. Schulz, and M.W. Wise

Center for Space Research
M.I.T.
Cambridge, MA 02139

J.J. Drake, J.Z. Juda, and M. Juda

Harvard-Smithsonian Center for Astrophysics
Cambridge, MA 02139

A.C. Brinkman, C.J.Th. Gunsing, and J. Kaastra

Space Research Organization of the Netherlands
Sorbonnelaan 1, 3584 CA Utrecht the Netherlands

G. Hartner and P. Predehl

Max-Planck-Institut für extraterrestrische Physik
Box 1603
D-85740 Garching Germany

ABSTRACT

The High-Energy Transmission Grating for AXAF was tested with the AXAF HRMA during December 1996 through April 1997 at NASA's MSFC X-Ray Calibration Facility. This first-use of the complete HETG spectrometer (HETGS) produced some low-level surprises in the Line Response Function (LRF) and indicate that the HETG is meeting or exceeding its resolving-power specifications.

This paper reviews the ingredients of the HETGS LRF, describes the pre-XRCF HETG sub-assembly measurements, presents an overview of the XRCF LRF-related measurements and data, and summarizes our knowledge of the HETG contribution to the HETGS Line Response Function. Two low-level effects, grating scatter and grating mis-alignment, were uncovered in this testing.

Keywords: AXAF, grating, calibration, X-ray, diffraction, scattering

1. INTRODUCTION

This paper is a status report on the analysis of data obtained at the X-ray Calibration Facility (XRCF) during the calibration of the Advanced X-ray Astrophysics Facility (AXAF) for about six months in 1996 and 1997. Only a portion of the total data collected is discussed in this paper; however, key results relevant to the spectral resolution and cross dispersion imaging properties of the AXAF High Energy Transmission Grating Spectrometer (HETGS) are presented.

The HETGS is the operational combination of the AXAF High Resolution Mirror Assembly (HRMA), the HETG grating, and the AXAF CCD Imaging Spectrometer (ACIS). The High Energy Transmission Grating on AXAF has been described previously in these conferences[1,2] and key aspects are summarized in a companion paper.[3] Additional instrument details are described as required in the discussions that follow.

Other author information: Send correspondence to HLM: Email: hermanm@space.mit.edu; Telephone: 617-253-8573; Fax: 617-253-0861 Up-to-date information available at: **http://space.mit.edu/HETG/xrcf.html**

The HETGS calibration requirements generally fall into two categories: calibration of the *Effective Area* and calibration of the *Line Response Function (LRF)*. This paper focuses on the calibration of the HETG contribution to the HETGS LRF; a companion paper[3] focuses on the HETG effective area measurements.

In the following sections, the definition and contributions to the LRF are described, our pre-XRCF measurements are summarized, the XRCF LRF measurement techniques are discussed, and finally the specific results we've obtained to date are presented.

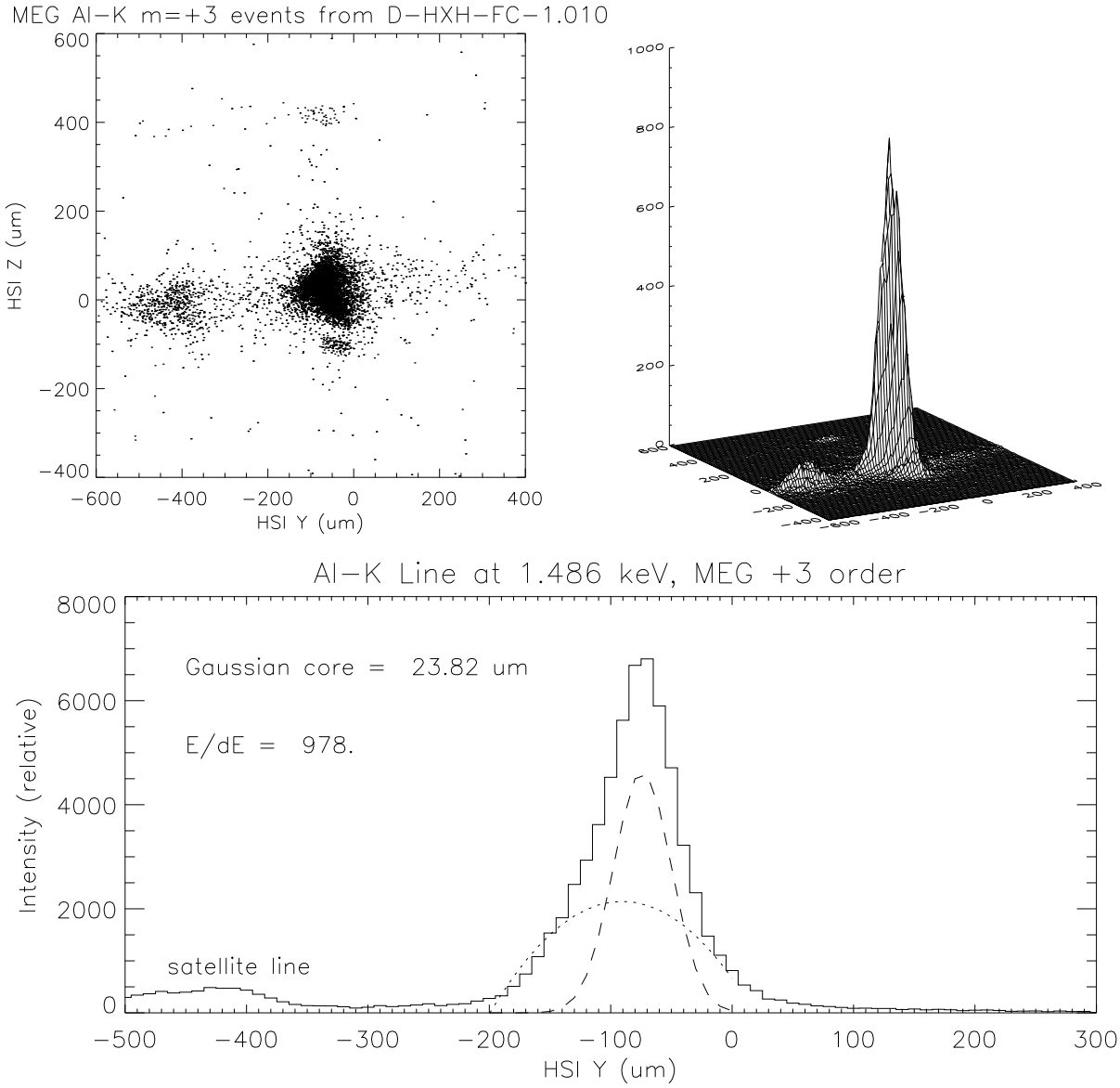

Figure 1. *PSF and LFR example. The event distribution (top left) may be described by a 2D point spread function PSF, $\rho(y,z)$ (top right). The resulting line response function LRF (lower plot) is shown with a Gaussian fit to its core.*

The events are from an XRCF HSI image of the 3rd-order MEG Al-K line; the HSI is centered at HSI_Y = 54.76 mm, HSI_Z = 4.496 mm. Visible in addition to the main peak is the "satellite line" at HSI_Y = -400. PSF outliers at HSI_Z = +400 and -100 represent mis-aligned grating facets.

2. THE HETGS LINE RESPONSE FUNCTION

2.1. LRF Definitions

The HETG, placed behind the HRMA, intercepts and diffracts the collected converging X-rays. As described in the companion paper[3] the focal plane image that results from a monochromatic near-axis point source can be considered as a set of images, one for each grating-order. These images are separated based on their diffraction angle given by simple diffraction theory[4]:

$$sin(\beta) = m\frac{\lambda}{p} \tag{1}$$

where m is the order of diffraction (an integer 0, $\pm 1, \pm 2$, ...), p is the grating period and β is the dispersion angle.

Each of these orders can be described by a *2-dimensional Point Spread Function (PSF)* which gives the normalized density of detected photons in the detector plane:

$$\rho(y,z) = P(y,z,E,m,dx,\phi,\theta,S(E,\alpha,\delta)) \tag{2}$$

where y,z are the detector coordinates, E,m are the energy and grating-order, dx is the telescope defocus, ϕ,θ are the location of the source with respect to the optical axis, and $S(E,\alpha,\delta)$ is the source surface brightness distribution at energy E. As an example, an X-ray event plot and the corresponding $\rho(y,z)$ PSF is shown in the upper plots of Figure 1 (this is data from XRCF and will be discussed in that context a little later.)

Because the spectroscopic information of a grating dispersive instrument is along the dispersion direction, it is useful to define the *one-dimensional Line Response Function (LRF)* to be the PSF integrated over the cross-dispersion direction:

$$l(y') = \int dz' P(y',z',E,m,dx,\phi,\theta,S(E,\alpha,\delta)) \tag{3}$$

where the y',z' indicate axes aligned with the dispersion and cross-dispersion directions in the detector plane. The lower plot in Figure 1 gives the LRF corresponding to the example PSF. Because of the image properties of the mirror, it is generally useful to (conceptually) break the LRF into at least two regions: a core or inner LRF and the wings or outer portion of the LRF.

The *Resolving Power* $R(E,m)$ of the spectrometer at energy E is defined as E/dE where dE is the full-width at half-maximum (FWHM) of the LRF. Typically the LRF core can be well fit by a Gaussian profile and in this case $dE \approx 2.35\sigma$.

2.2. LRF for the Faceted Rowland Geometry

The HETG is a faceted Rowland torus design and has been engineered and built to accurately place each facet at its prescribed location and orientation. Although analysis of the image produced by this Rowland design can be quite complex,[5] the basic features can be understood through simple ray geometry.

In the "Top View" of Figure 2 we are looking along the cross-dispersion direction, z'. The diffraction angle is β, which through the geometric properties of the circle, causes rays diffracted from gratings located on the Rowland circle to converge at another point on the Rowland circle. The dotted lines represent zero-order ($m = 0, \beta = 0$) rays and the solid lines a diffracted order ($m > 0, \beta > 0$). The bottom panel, "Side View", looks along the dispersion direction, y', at rays from a set of gratings arranged perpendicularly to those above.

Together, these constructions show the astigmatic nature of the spectrally focussed image: the rays come to a focus in the dispersion direction, the *Rowland focus*, at a different location from their focus in the cross-dispersion direction, the *Imaging focus*. In order to maintain the best spectroscopic focus the detector surface must conform to or approximate the Rowland curvature.

At the Rowland focus the image is elongated (blurred) in the cross-dispersion direction by a peak-to-peak value given by similar triangles as:

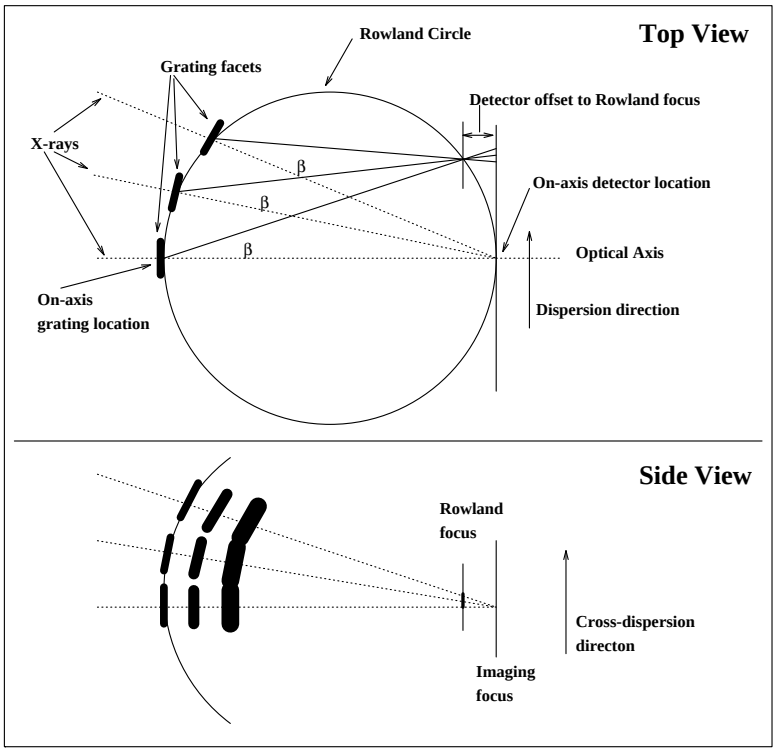

Figure 2. *Simplified ray geometry for the Rowland torus design. The two views are orthogonal to each other and show the gratings on the surface of a torus. Please see the text for a detailed explanation.*

$$\Delta z' = \frac{2R_0}{X_{\rm RD}}\beta^2 X_{\rm RD} \tag{4}$$

where R_0 is the distance of the ring of gratings from the optical axis and $X_{\rm RD}$ is the Rowland spacing; the $X_{\rm RD}$ is not cancelled to explictly show the term $\beta^2 X_{\rm RD}$ – the distance between the Rowland and Imaging focus locations.

It is important to note that in the ideal case the grating provides primarilly a deflection to the rays being focussed by the HRMA. Because of this, the focus quality is not dramatically effected by perturbations of the grating geometry from the ideal Rowland Torus design. In particular, the flight HETG is built to a Rowland diameter of 8635 mm, yet at XRCF because of the finite source distance changes to the HRMA focal length and other considerations, the HETG Rowland spacing (on-axis grating to detector distance) was 8782.8 mm. This difference adds an insignificant additional spectral blur (of order 1 μm rms.)

2.3. Error Budget and Ray-Trace Studies

The design of the HETG involved the use of an error budget to sum the various contributions to the resolving power. The error budget terms were verified by performing simplified ray-traces of single and multiple facets. The pre-XRCF conservative resolving power expectations are plotted in Figure 3.

In addition to the mirror PSF and the astigmatic cross-dispersion blur, there are two main error terms which depend on how well the HETG is built i) period variations within and between facets ("dp/p") and ii) alignment variations ("roll" about the normal to the facet surface) within and between facets. The period variations lead to additional blur in the dispersion direction:

$$dy' \approx \beta X_{\rm RD}\frac{dp}{p} \tag{5}$$

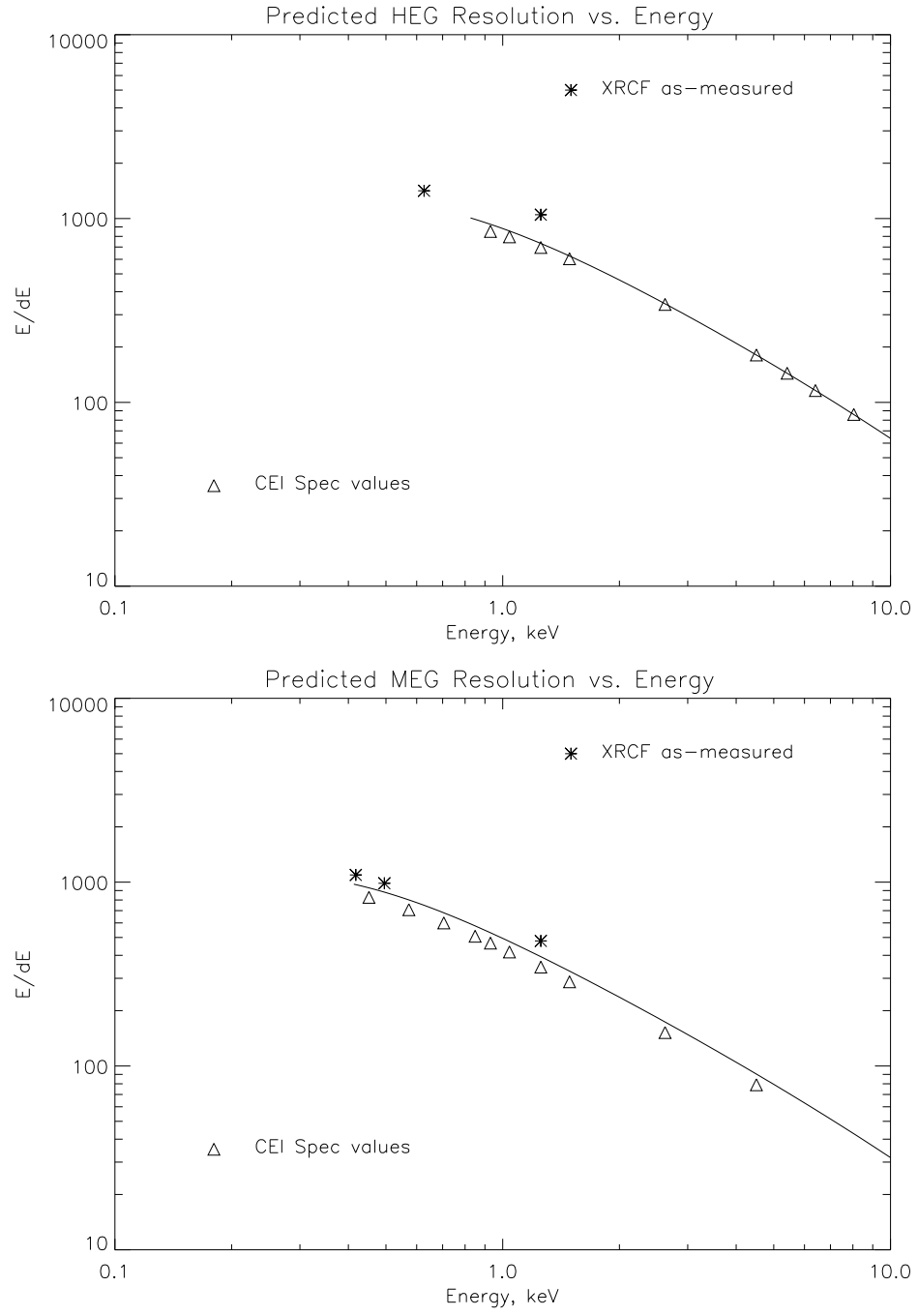

Figure 3. *Spectral resolving power for the HEG and MEG spectra of the HETGS. The resolving power E/dE is plotted vs. energy. The triangles are specifications to be met and the solid lines are our pre-XRCF conservative error budget expectations. The asterisks represent as-measured values at XRCF for $E = 1.254$ keV at HEG+1, HEG+2, MEG+1, MEG+3 and for $E = 1.486$ keV at MEG+3; the measurements at higher order ($|m| > 1$) are plotted at the energy $E/|m|$.*

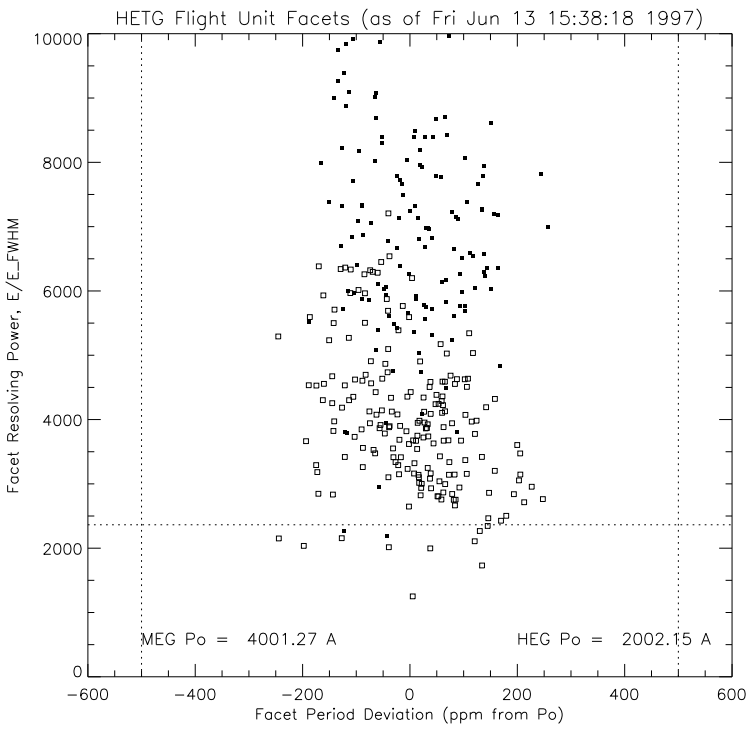

Figure 4. *Period measurements of the 336 HETG flight grating facets. The Facet-to-facet period variations and internal period variations lead to dp/p values of < 150 ppm compared to the 250 ppm used in the conservative error budget.*

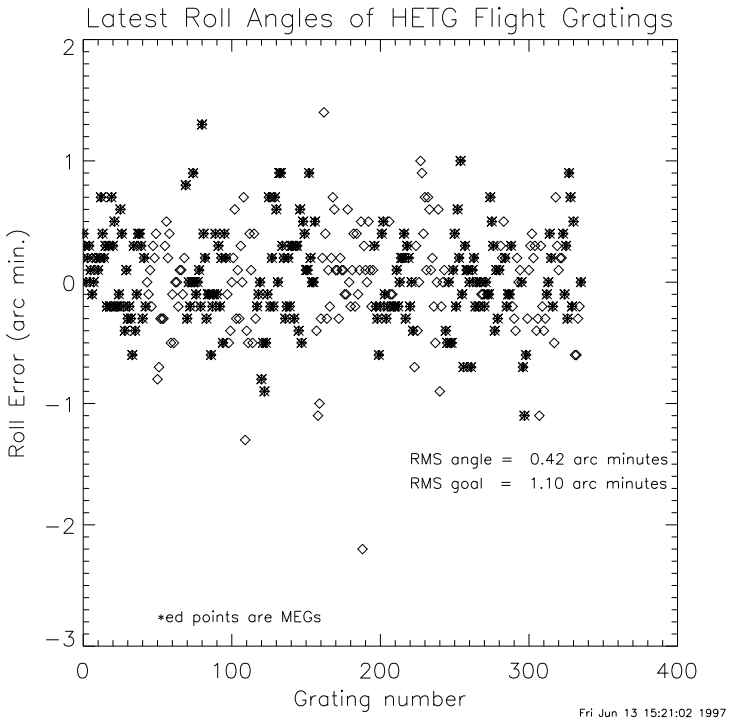

Figure 5. *Measured roll errors for the 336 flight gratings. The rms value $\gamma = 0.42$ arc minutes is well below the specification of 1.1 arc minutes.*

where dy' and dp/p are rms quantities. The roll errors lead to additional blur in the cross-dispersion direction through the equation:

$$dz' \approx \beta X_{\rm RD} \gamma \tag{6}$$

where dz' and γ are rms values in units of mm and radians respectively.

3. PRE-XRCF FACET MEASUREMENTS

As the discussion above points out, the key facet-level parameters that effect the HETGS LRF are the grating period variations (both within and between facets) and the grating alignment, or "roll", variations (again within and between facets). The facet period, period variations, and roll variations were measured using a Laser Reflection setup, described in Dewey *et al.*.[6] The expected HETG equivalent dp/p is expected to be less than 150 ppm rms for both HEG and MEG gratings based on the data summarized in Figure 4.

The facet-to-facet alignment variations were measured as part of the facet installation procedure; the roll angle of each facet with respect to a reference facet was measured in the HETG Alignment Facility based on the polarization alignment technique of Anderson *et al.*.[7] The total roll variation of the facets is measured with the polarization technique to be well below our design specification of 1.1 arc minutes rms, Figure 5.

4. XRCF LRF MEASUREMENTS AND PRELIMINARY RESULTS

4.1. XRCF Hardware

In this section we mention the XRCF hardware properties and techniques that allow precise LRF measurments. For the general layout and features of the XRCF hardware see the companion paper[3] where the two operational phases are also described as well as the method by which tests were specified and executed.

During Phase I calibration the HSI detector[8] provided imaging capability at high event rates, for example the image in Figure 1. The HSI also was fitted with a mask with a "cusp" to allow the bright PSF core to be occulted while the surrounding wings of the PSF were observed.

The FPC and SSD detectors[9] could have a slit aperture selected for use - in this way a direct measurement of the 1D LRF was possible.

Extensive LRF tests could be performed with the ACIS-2C detector given its (non-flight) high event-rate readout.

During Phase II calibration the flight detectors were present. Because LRF tests generally require well focussed beams and given the HRC pore extraction limits and the ACIS telemetry limits, extensive LRF studies were not in general carried out – the exception being enough data with ACIS-S to allow us to verify the Rowland curvature of the CCDs.

4.2. Summary of HETG XRCF Measurements

Tables 1,2 provide a summary of all LRF-related data taken at XRCF with the HETG inserted in the optical path and an indication of their use and data volume (number of measurements.) The various types of tests are mentioned in the following sections where preliminary results are included.

4.3. Focus tests

The focus tests (Focus Check FC and Shutter Focus SF) were performed by cycling through the quadrants of the mirror. When examining the 0th order, the inner shells were closed for images of the MEG 0th order and opened (while closing the outer shell pair) for the HEG 0th order measurement. The displacement of the image centroids gave an estimate of the detector defocus using a simple thin lens approximation and the knowledge that the detector was already placed within 0.5 mm of the desired focus position. The insertion of gratings was not expected to have an effect on detector focus location, and this was observed to the measurement accuracy of about 25 microns. Furthermore, once the fixed offset of about 180 microns was corrected, an additional defocus measurement gave an answer consistent with zero defocus error. All 0th order images were shaped as bowties or hourglasses, depending on the set of open shutters, as expected, due to mirror scattering, which redistributes photons preferentially perpendicular to the scattering surface.

Table 1. Table of LRF related HETG XRCF Measurements in Phase I.

Type	Detector[a]	
	FPC/SSD	HSI
FC and SF	-	Verify focus, check PSF [16]
dFocus	-	Defocus and in-focus images [2]
Alignment	-	Gross vignetting, mis-aligned gratings [3]
PSF/1D	LRF core, wings [21]	-
PSF/Outer	-	Wings, scatter [8]
3D (Offaxis)	-	Offaxis images [6]

[a] The number of tests is given in brackets.

Table 2. Table of HETG XRCF Measurements in Phase II.

Type	Detector[a]		
	ACIS-2C	HRC	ACIS
FC and SF	Verify/check focus [7]	Verify/check focus [1]	-
dFocus	Find best focus [10]	-	-
PSF/Inner	Core, wings; offaxis images [23]	-	Core, wings; offaxis images [8]
Scattering	Wings, scatter [5]	-	Grating scatter, pileup effects, readout modes (, effective area) [7]

[a] The number of tests is given in brackets.

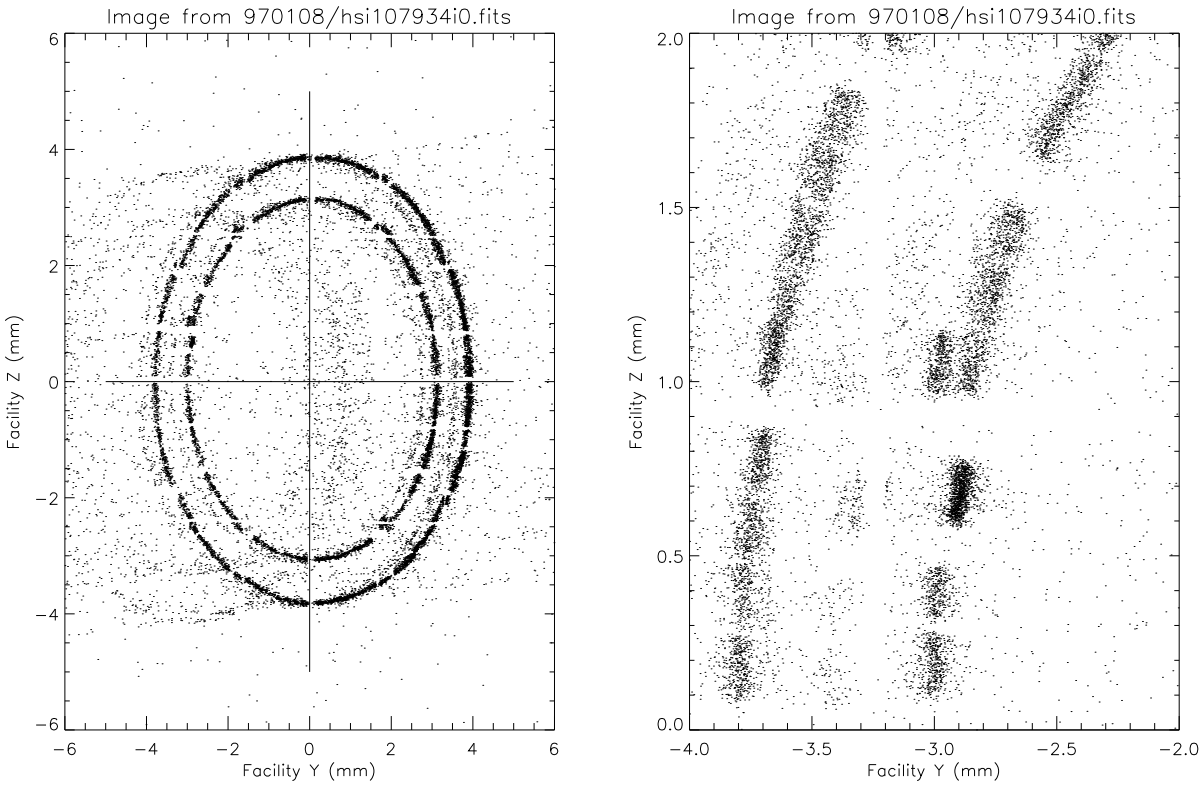

Figure 6. *Defocussed HSI image of the MEG Al-K 3rd order. Individual grating facets are visible here in the two MEG rings of gratings. At right a blowup shows mis-aligned facets by the jumbling of the facet images.*

4.4. Cross Dispersion Images

Higher order images were examined in order to verify the placement of the gratings and detectors on the Rowland circle. The detector was offset by the amount appropriate to the Rowland circle and a shutter focus was performed.

Surprisingly, the images of MEG Al-Kα in third order showed several additional images at the same dispersion distance as the Al-Kα line, these are the weak features at +400 and -100 in HSI Z seen in Figure 1. The images individually were 2-6% of the power in the main image. Several of the images were displaced in the cross-dispersion direction by 120 microns and a fourth deviated by almost 400 microns, corresponding to rotations of the dispersion direction by 7 arc minutes and 24 arc minutes, respectively. Such large rotations were not expected, based on subassembly measurements (*e.g.*, Figure 5) so an additional test was devised to confirm this possibility.

A defocussed image of the MEG +3 order Al-K line (Alignement test) reveals the individual facets, Figure 6. A grating mis-aligned in roll will show up as having its image shifted along the z' axis – this can be seen for the "400 μm offender" at around coordinates Y = -3 mm, Z = +1 mm where the regular set of grating images is jumbled. By analyzing this image 6 gratings were found to be misaligned by 5 to 23 arc minutes. All of these were from a single fabrication lot. Further tests have confirmed that fabrication irregularities produced excess stress gradients in the grating polyimide support structure leading to inaccurate polarization alignment measurement values. These "mis-aligned gratings" will be explicitly included in our instrument model.

4.5. Spectral Resolution

The direct approach to resolution measurement would be to use an X-ray source with an intrinsically narrow line at low energy. The best candidate emission line for this function was the Mg-Kα line at 1.253 keV. Lower energy K lines have resolvable natural line widths (e.g. O-K or C-K) and the L lines (of Ti, Fe, and Ni, for example) were generally much weaker and substantially more complex. Therefore, we used an indirect approach, observing the higher energy

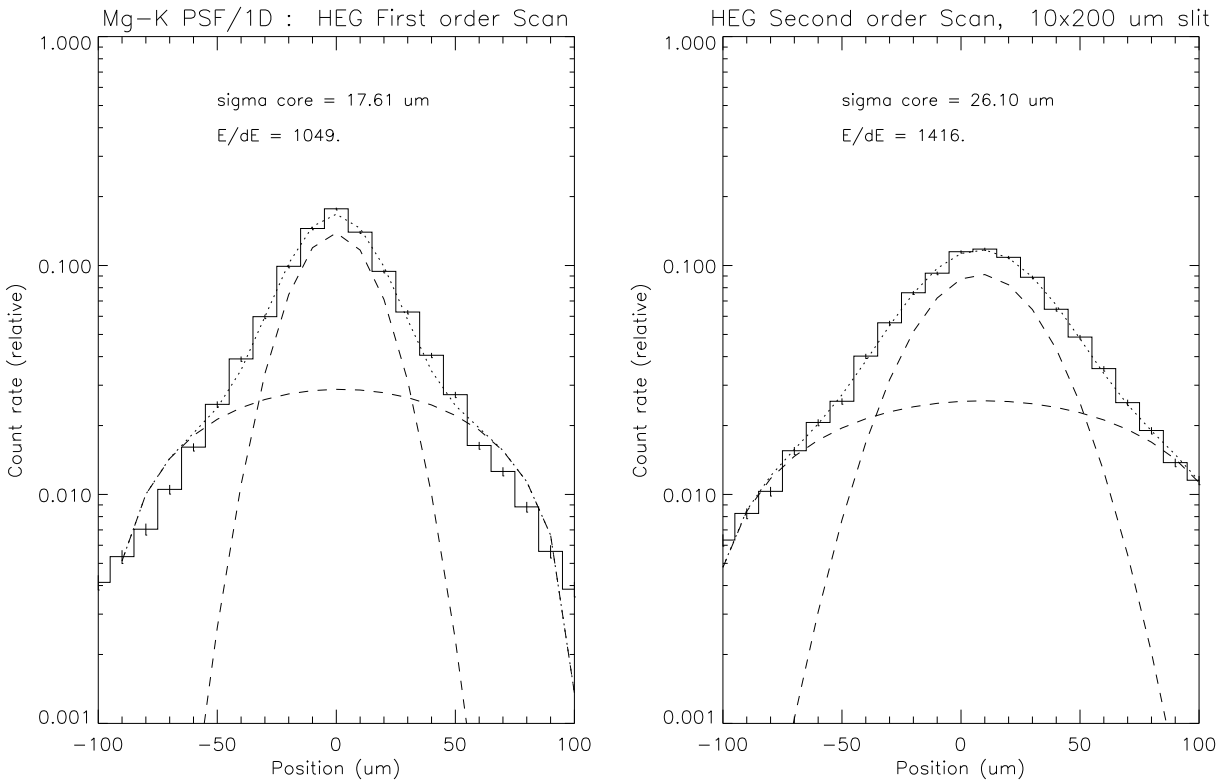

Figure 7. *Slit scans with the FPC across Mg-K HEG 1st and 2nd orders. Gaussian approximations to the cores indicate high resolving powers are being achieved.*

K lines at high order. Using a 200 μ m by 10 μ m slit, the HEG+1, HEG+2, MEG+1, and MEG+3 images were scanned directly ("PSF/1D" measurement) to measure the LRF. Figure 7 shows the data and a simple fit for the HEG orders.

4.6. Scattering or Incoherent Diffraction

A test series was developed to search for near line scattering wings (PSF/Outer, Scattering) that would be a concern when measuring absorption features near bright lines. The Double Crystal Monochromator (DCM) was tuned to the bright line W-Mα at 1.775 keV in the anode spectrum. The current was turned to the lowest possible value to get a count rate for the total line and then the current was turned to the highest possible value for the scattering test. The image was placed on a detector mask "cusp", in order to block the core of the image but allow photons beyond $E/100$ of the target line. Mirror scattering was expected but would be azimuthally symmetric, while grating line scatter was expected preferentially along the direction of dispersion, so would be distinguishable from mirror scattering. After a long integration at high current, a total of 100,000 counts would be obtained from the core of the line (without the blocking cusp), so the test could detect scattered power levels below 0.1% of peak.

The result, Figure 8, was somewhat surprising at the time: although there was no obvious evidence for power along the dispersion direction near the line, there were clearly significant events dispersed 1-10 mm from the line. In order to verify that the DCM had no significant spectral leakage that could cause the observed effect, we tuned the DCM off of the bright line by only 15 eV. The DCM resolution at 1.775 keV is about 5 eV, so very little power was expected and the current was turned up to its maximum setting. There were no events at the expected dispersion location of 1.775 keV, indicating that it had been suppressed at a level better than one part in 10^5. We concluded, therefore, that the gratings were incoherently diffracting a modest fraction of the line emission to large dispersion distances. This fraction was estimated at 0.4% over a 10 mm span.

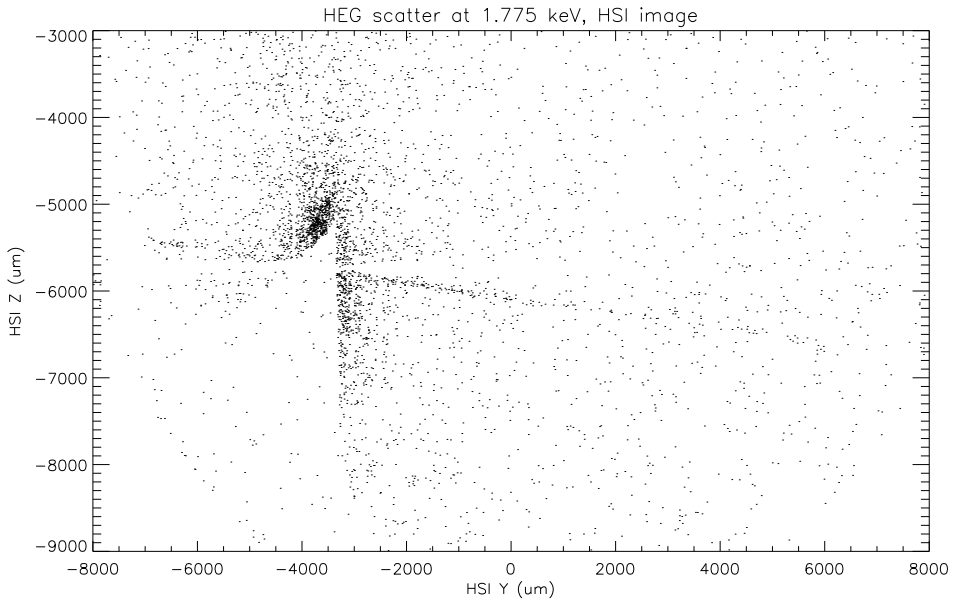

Figure 8. *Phase I HEG scatter test. The core of the HSI image of the DCM monochromatic 1.775 keV line in HEG first order is blocked by the HSI cusp. Extending from the cusp along the HEG dispersion axis are scattered 1.775 keV photons. Of order 0.4% of the line flux is scattered.*

Subsequent modelling and further tests indicated that minor bar location variations could cause an incoherent redistribution of monochromatic light. The grating-bar variations needed can be quite small, of order 10% of the the distance between bars.

5. SUMMARY

The complete analysis of all XRCF data pertaining to the HETGS LRF is an on-going project. However, at this point, we believe that i) we have identified all major differences between the ideal and as-built HETG and ii) the HETGS will perform at or above its design specifications.

6. ACKNOWLEDGEMENTS

To the full cast and crew of XRCF testing we offer and share a hearty "Congratulations!". In particular we thank Project Science, TRW, MSFC, Buddy Randolph, EK, MST, the AXAF Science Center, and the ACIS and HRC teams.

From an HETG perspective we additionally acknowledge the efforts of Mike McGuirk, Pat Hindle, Dick Elder, Chris Pak, Rich Aucoin, Ed Warren, and Bob Laliberte to get HETG to XRCF as well as providing understanding of HETG-XRCF alignments and data.

This work was supported in part by NASA under the HETG contract NAS-38249 and the AXAF Science Center contract to the Smithsonian Astrophysical Observatory, NAS8-39073.

REFERENCES

1. Canizares, C.R., Schattenburg, M.L., and Smith, H.I., "The High Energy Transmission grating Spectrometer for AXAF", in *X-ray Instrumentation in Astronomy, Proc. SPIE*, Vol. **597**, 253–260 (1985).
2. T.H. Markert, C.R. Canizares, D. Dewey, M. McGuirk, C. Pak, and M.L. Schattenburg, "The High Energy Transmission Grating Spectrometer for AXAF", *EUX, X-Ray, and Gamma-Ray Instrumentation for Astronomy V*, Proc. SPIE, Vol. **2280**, 168–180 (1994).

3. D. Dewey, H.L. Marshall, K.A. Flanagan, C. Baluta, C.R. Canizares, D.S. Davis, J.E. Davis, T.T. Fang, D.P. Huenemoerder, J.H. Kastner, N.S. Schulz, M.W. Wise, J.J. Drake, J.Z. Juda, M. Juda, A.C. Brinkman, T. Gunsing, J. Kaastra, G. Hartner and P. Predehl, "Towards the Callibration of the HETG Effective Area", *these proceedings*, (1997).
4. M. Born and E. Wolf, *Principles of Optics, Sixth Ed.*, pp. 401-414., Pergamon, New York, 1980.
5. Beuermann, K.P., Brauninger, H., and Trumper, J., *Applied Optics*, Vol. **17**, no. 15., 2304 (1978).
6. D.Dewey, D.N. Humpheries, G.Y. McLean and D.A. Moschella, "Laboratory Calibration of X-ray Transmission Diffraction Gratings", *EUX, X-Ray, and Gamma-Ray Instrumentation for Astronomy V*, Proc. SPIE, Vol. **2280**, 257–271 (1994).
7. E.H. Anderson, A.M. Levine, and M.L. Schattenburg, "Transmission X-ray Diffraction Grating Alignment using a Photoelastic Modulator", *Applied Optics*, Vol. **27**, pp. 3522-3525 (1988).
8. I.N. Evans, E.M. Kellogg, W.C. McDermott, M.P. Ordway, J.M. Rosenberg, and B.J. Wargelin, "High Speed Imager AXAF Calibration Microchannel Plate Detector", *these proceedings*, (1997).
9. B.J. Wargelin, E.M. Kellogg, W.C. McDermott, I.N. Evans, and S.A. Vitek, "AXAF Calibration: The HXDS Flow Proportional Counters", *these proceedings*, (1997).